Trans Indian Inst Met (2020) 73(3):675–689
https://doi.org/10.1007/s12666-020-01868-1

ORIGINAL ARTICLE

Welding L415/316L Bimetal Composite Pipe Using Post-Internal-Welding Process

Liying Li[1] · Jun Xiao[1] · Bin Han[1] · Cong Zhou[1] · Xiaolei Wang[1]

Received: 30 June 2019 / Accepted: 17 January 2020 / Published online: 10 February 2020

Abstract The butt welding of bimetal composite pipes generally adopts single-side welding, which easily gives rise to the problems such as high cost or crack initiation. In this paper, the butt welding of L415/316L bimetal mechanical lined pipes was conducted using post-internal-welding process, which is double-side welding process, proposed by the authors. Firstly, the effect of groove shape on the weld process was discussed. Then, microstructures and mechanical and corrosion-resistance properties of welded joints welded using two different welding materials, 309MoL and 309L, were investigated. The results show that the most suitable groove is that L415 is V shape with angle of 60° and blunt edge of 1 mm and 316L is stripped 6–8 mm. The weld of both 309MoL and 309L is composed of austenite and a small amount of ferrite, but the presence of Mo can refine the grains and increase the content of ferrite phase. The width of transition layer is about 0.6–0.8 mm located at the weld junction of stainless steel weld and carbon steel weld, and the transition layer mainly contains martensite. The tensile and bending performances of the welded joints using both 309MoL and 309L do meet the standard requirements. The welding wire 309MoL can improve the corrosion resistance to Cl^- compared to 309L. It is advisable to use the post-internal-welding process and 309MoL for the welding of bimetal composite pipes under environments containing Cl^-.

Keywords L415/316L bimetal mechanical lined pipe · Post-internal-welding process · Groove shape · Welding materials · Microstructure · Corrosion resistance

1 Introductions

Recently, with the great consumption of petroleum resources and the depletion of large conventional oil–gas fields, the exploration and development of oil–gas fields are moving toward areas with harsh environmental conditions such as environment with deep wells, deep seas, high temperature and high pressure. These environments are often accompanied by highly corrosive elements such as CO_2, Cl^-, and H_2S [1–3]; so the corrosion resistance requirement of pipeline materials used for exploitation and transportation has increased. Although the traditional methods of both adding corrosion inhibitor and coating anticorrosion can resist corrosion to a certain extent, it is easy to cause failure for the carbon steel pipes. Corrosion-resistant alloy (CRA) pipes have superior corrosion resistance, but they are not widely used because of their high costs. In addition, non-metallic pipes do not meet the requirements of engineering application due to their low rigidity and strength as well as poor impact resistance performance [4]. The research data at home and abroad have shown that the use of bimetallic composite pipes is one of the effective ways, which are relatively safe, economic and reliable, to solve the oil–gas exploitation and transportation under severe corrosion conditions [5–7].

The bimetal composite pipes are composed of both the outer thick layer of carbon steel (low alloy steel) and inner thin CRA layer [8, 9]. They combine the excellent mechanical properties of the outer layer and the good corrosion resistance of the inner layer, and their price is

✉ Liying Li
llying3456@163.com

[1] School of Materials Science and Engineering, China University of Petroleum, Qingdao 266580, Shandong, China

about 50% of the CRA pipes [10]. The bimetal composite pipes are divided into bimetal mechanical lined pipes and metallurgical clad pipes. The former is lower in cost and has wider applications compared with the latter. So, bimetal composite pipes have been developed rapidly in the field of oil, natural gas, chemical and electric power industries [4, 11].

However, the weldability of the bimetal composite pipes is not desirable due to the large difference in physical properties between the base pipe and the inner pipe, and some problems tend to occur, such as cracking and low corrosion-resistance after welding. The occurrence of cracks is closely related to large weld residual stresses which is generated due to the mismatching of materials [12]. Jiang et al. [13] studied the weld residual stress in a clad plate by neutron diffraction and finite element method. The diameter of bimetal composite pipes is generally less than 660 mm, so the welding of bimetal composite pipes usually adopts single-side welding, and the welding sequence is inner layer (backing welding)–transition layer (transition welding)–outer base layer (filler and capping welding) [14–19]. There are currently two welding materials. On the one hand, all weld beads, including backing welding, transition welding, and filler and capping welding, adopt CRA welding materials. On the other hand, mixed welding materials are used, that is, CRA wire is used for the backing welding and transition welding, and the equal-matching carbon steel welding material is used for the filler and capping welding. The problems when using CRA welding materials are low welding efficiency, high welding costs and low weld strength. But for the mixed welding materials, they have not yet been widely used because that the hardened microstructure layer may cause cracks at the location between the transition and filler welding of outer carbon steel layer in the bending test. The existence of cracks is related to the thickness of hardened microstructure layer. However, there have been few studies on how to reduce the thickness of hardened microstructure while improving welding efficiency and reducing welding costs.

Therefore, the post-internal-welding process, which is according to a new welding sequence where the outer carbon layer is welded prior to the inner stainless layer, has been proposed by the authors, and its advantages include thin hardened microstructure layer, high welding efficiency and low welding costs. This article used post-internal-welding process for the butt welding bimetal lined pipe L415/316L. Firstly, four groove shapes were designed. Then, the welded joints were completed using two different welding materials. The microstructure, mechanical properties and corrosion behavior of the welded joints were investigated.

2 Experimental Material and Procedures

2.1 Experimental Materials

The base metals employed are bimetal lined pipe L415/316L with the outer diameter of 355 mm. The outer base layer is L415 with thickness of 11 mm, while the inner layer is 316L with thickness of 2 mm. The chemical compositions of base metals and filler metals are investigated using the optical emission spectrometer and are reported in Table 1. The mechanical properties of both base metals [20, 21] and weld metals provided by the supplier are shown in Table 2. In order to ensure the corrosion resistance of 316L layer, considering the burning of alloying elements, welding materials with higher contents of Cr and Ni than 316L are generally selected, so 309L and 309MoL welding wires are adopted in this case. But for the welding of L415 layer, equal-strength matching materials of ER70S-6 and ER5015 are used.

2.2 Welding Parameters and Procedures

2.2.1 Groove Design

Four groove shapes are designed, as shown in Fig. 1. Groove A is double V shaped, the V-shaped angle of L415 with blunt edge of 2 mm is 60°, and the V-shaped angle of 316L is 90°. Groove B is outer-V and inner-concave shape, the groove of L415 is V shaped with angle of 60° and blunt edge of 2 mm, and both L415 with thickness of 2 mm and 316L are stripped 4 mm. Groove C is similar to groove A except that the V-shaped groove of 316L includes L415 with thickness of 1 mm, while the blunt edge of L415 is 1 mm. Groove D is similar to groove B except that the blunt edge of L415 is 1 mm and 316L is stripped 8 mm. After welding test, initially, the weld appearance is observed. Secondly, if the weld appearance is fine, the radiographic testing (RT) is measured. Finally, the best groove shape is chosen for the butt welding bimetal lined pipe L415 /316L.

2.2.2 Welding Sequence and Parameters

The welding sequence is shown in Fig. 2. The post-internal-welding process has been used for the butt welding of L415/316L pipes. The welding sequence is that, the L415 layer is welded prior to the 316L layer. For the grooves A and B, the special welding sequence is as follows: Firstly, the root welding (1st) of L415 layer is carried out using manual gas tungsten arc welding (GTAW). Secondly, the filler welding (2nd and 3rd) of L415 layer is carried out using manual shielded metal-arc welding (SMAW).

Table 1 Chemical compositions (mass fraction, %)

	C	Mn	Si	S	P	Cr	Cu	Ni	Mo	V	Fe
Base metals											
L415	0.15	1.50	0.40	0.001	0.020	0.05	–	0.02	0.02	–	Balance
316L	0.004	1.129	0.640	0.000	0.045	16.316	–	10.028	2.035	–	Balance
Filler metals											
ER70S-6	0.08	1.44	0.8	0.0062	0.015	0.014	0.056	–	0.001	0.0017	Balance
ER5015	0.111	0.341	0.541	0.009	0.019	0.0003	–	0.014	0.006	0.003	Balance
ER309L	0.02	1.9	0.37	0	0.022	23.11	–	13.76	–	–	Balance
ER309MoL	0.02	0.8	0.40	0.001	0.018	24	–	13.50	2.7	–	Balance

Table 2 Mechanical properties of base metals [20, 21] and filler metals

	Tensile strength R_m/MPa	Yield strength R_{eL}/MPa	Elongation A/%	Charpy energy K_{V2}/(J/°C)
Base metals				
L415	≥ 520	415–565	≥ 18	–
316L	≥ 485	≥ 170	≥ 30	–
Filler metals				
ER70S-6	545	445	31	97.7/− 30
ER5015	550	440	30	140/− 30
ER309L	620	–	41	121/− 60
ER309MoL	645	–	37	92/− 60

Thirdly, the filler (4th) and capping (5th) welding of 316L layer are finished using manual GTAW. Finally, the capping (6th) weld of L415 layer is welded using manual SMAW. For the grooves C and D, the special welding sequence is similar to that of grooves A and B except that sealing welding (1st and 2nd) is added before the butt welding. The sealing welding also adopts GTAW. For the welding of L415 layer, the single-layer single-pass welding has been used. But for the welding of 316L layer, according to the size of the groove, both single-layer single-pass welding and single-layer multi-pass welding have been used. The designed welding parameters for grooves A and B are listed in Table 3, and those for grooves C and D are listed in Table 4. The argon with a purity of 99.99% is used as the protective gas of GTAW, and its flow rate is 8–15 L/min. The polarity of welding current for GTAW is direct current electrode negative (DCEN). There are two advantages for using DCEN. On the one hand, the arc is stable. On the other hand, tungsten is the cathode, and the heat is concentrated on the base material, which can extend the life of the tungsten electrode.

2.2.3 *Microstructure and Properties Analysis*

After welding test, the tensile and bending properties of the welded joint are tested, according to the standards of GB/T 2651-2008 (tensile test method on welded joints) and GB/T 2653-2008 (bend test methods on welded joints), respectively, and schematic diagrams of the tensile and bending samples are shown in Fig. 3. The bending angle is 180°. The hardness is measured at a load of 200 g and dwell time of 15 s. The chemical immersion method has been used to measure the pitting corrosion resistance of the weld bead of 316L layer according to the standard GB/T 17897-2016 (corrosion of metals and alloys—corrosion test for pitting corrosion resistance of stainless steels in the ferric chloride solution). The corrosion solution is 6% $FeCl_3$ solution. The test temperature and time are 50 °C and 24 h, respectively. The microstructures are observed by an optical microscope (OM) and electron backscattered diffraction (EBSD). The chemical compositions have been analyzed by energy-dispersive spectroscopy (EDS) attached to a scanning electron microscope (SEM). Fractography of the tensile samples is observed by SEM.

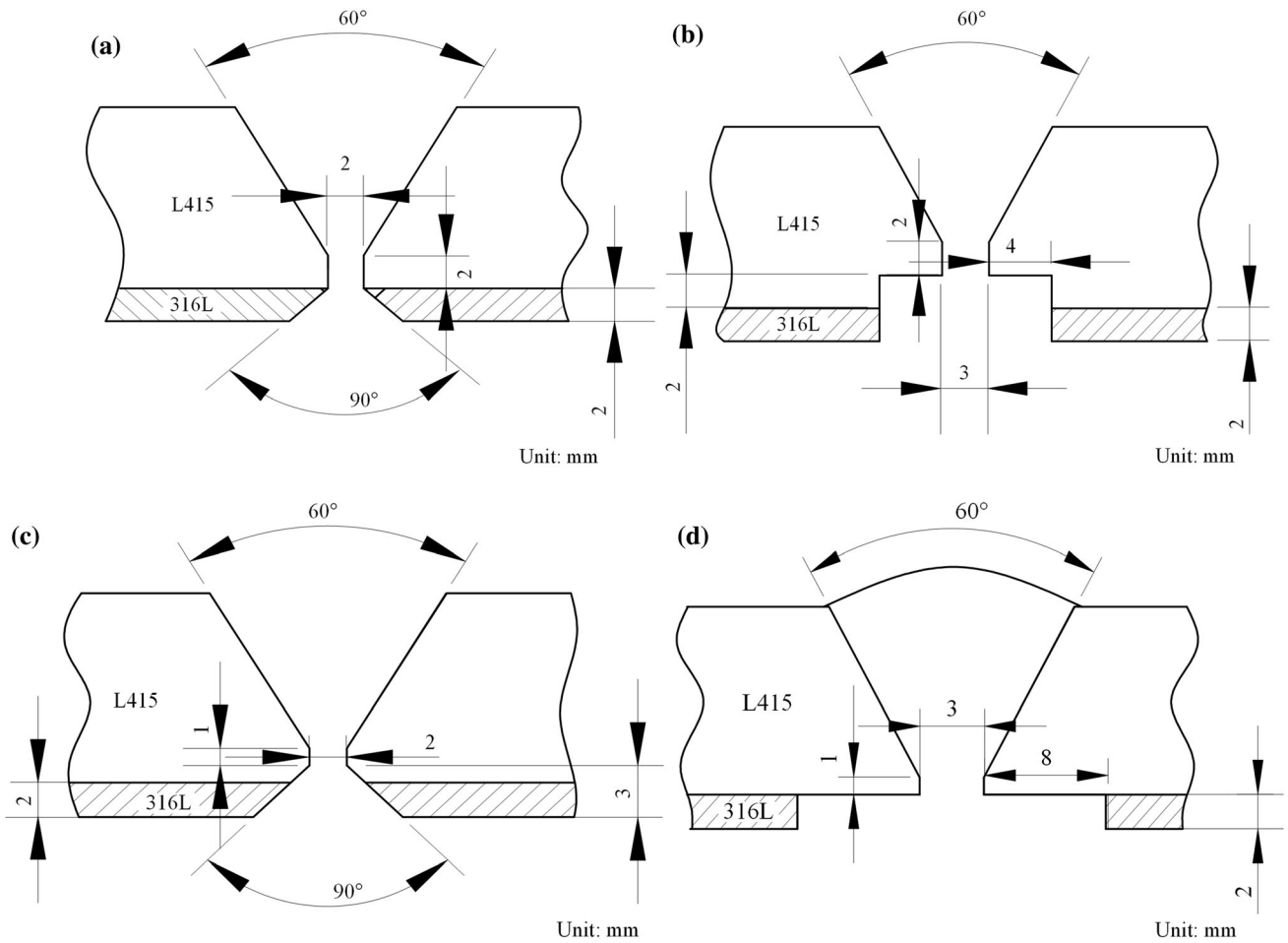

Fig. 1 Groove shapes **a** groove A; **b** groove B; **c** groove C; **d** groove D

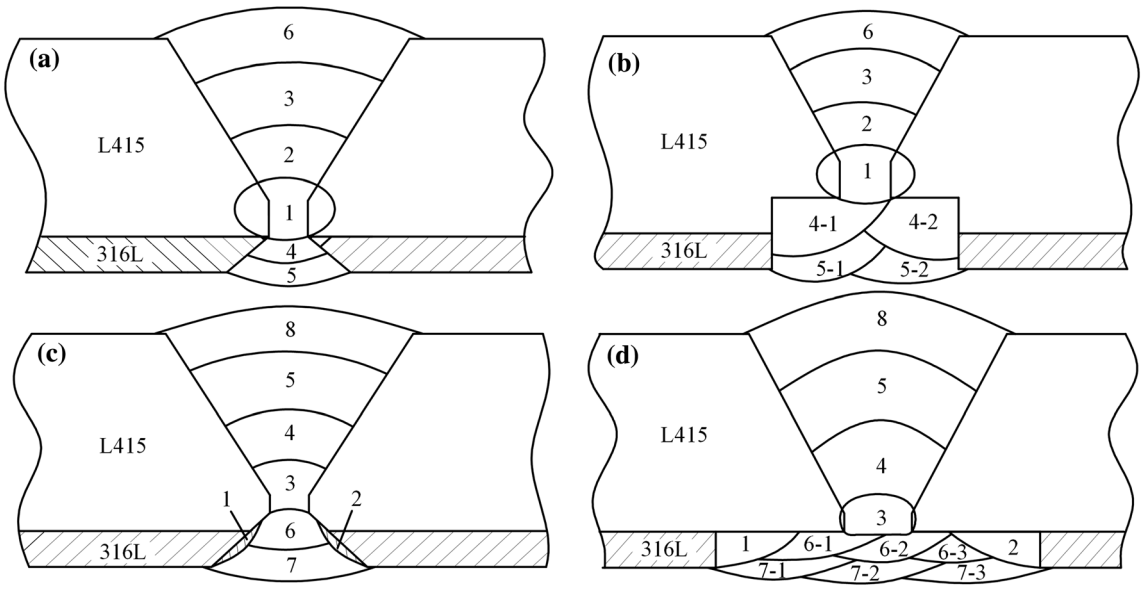

Fig. 2 Welding sequence **a** groove A; **b** groove B; **c** groove C; **d** groove D

Table 3 Designed welding parameters for grooves A and B

Weld bead/weld layer	Welding process	Filler metals		Electrical characteristics		Welding voltage (V)	Welding speed (cm/min)
		Welding materials	Diameter (mm)	Polarity	Welding current (A)		
1	GTAW	ER70S-6	ϕ2.5	DCEN	100–130	20–28	3–8
2–3	SMAW	E5015	ϕ3.2	DCEP	100–150	20–28	5–12
4–5	GTAW	ER309L	ϕ2.4	DCEN	100–150	8–14	3–8
6	SMAW	E5015	ϕ3.2	DCEP	100–150	20–28	5–12

Table 4 Designed welding parameters for grooves C and D

Weld bead/Weld layer	Welding process	Filler metals		Electrical characteristics		Welding voltage (V)	Welding speed (cm/min)
		Welding materials	Diameter (mm)	Polarity	Welding current (A)		
1–2	GTAW	ER309L	ϕ2.0	DCEN	60–80	20–25	3–8
3	GTAW	ER70S-6	ϕ2.5	DCEN	100–130	20–28	3–8
4–5	SMAW	E5015	ϕ3.2	DCEP	100–150	20–28	5–12
6–7	GTAW	ER309L	ϕ2.0	DCEN	100–150	8–14	3–8
8	SMAW	E5015	ϕ3.2	DCEP	100–150	20–28	5–12

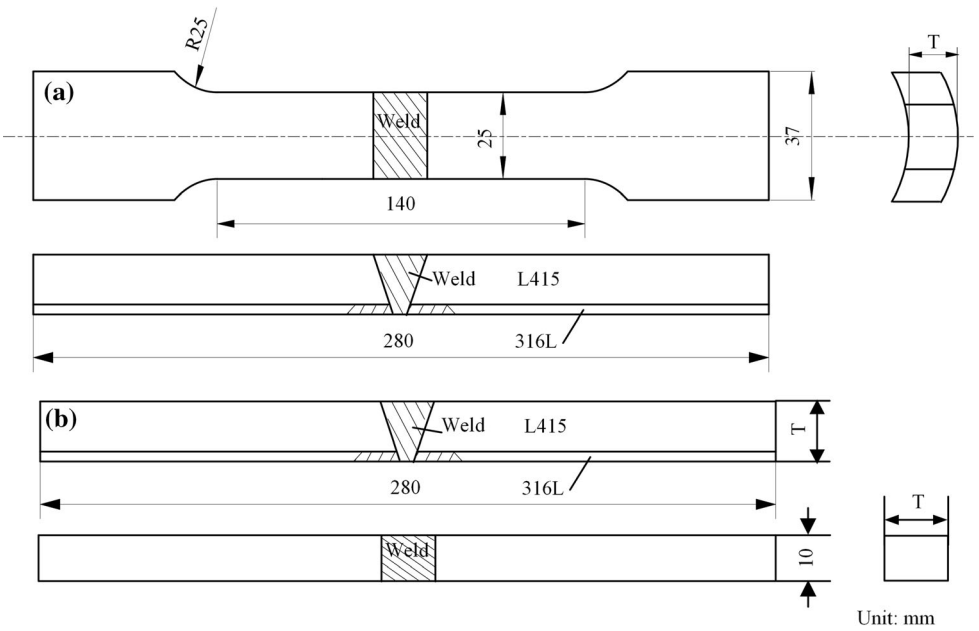

Fig. 3 Schematic diagrams of tensile and bending samples

3 Results and Discussion

3.1 Effect of Groove Shape on Welding Process

For groove A, its advantage lies in two aspects. On one hand, the cutting amount of 316L is small, so the filler metal of the stainless steel is less and correspondingly the production costs are low. On the other hand, the groove processing is convenient, so the production time can be shortened and the production efficiency can be improved. But there are two issues that need attention. One is that, the current of 4th and 5th weld bead should be reduced properly in order to reduce the fusion ratio to ensure the corrosion resistance of the welded joints. Other is that, the root (1st) weld bead should avoid the contact with 316L, so small welding current and low welding speed should be

adopted for root (1st) weld. However, test results show that the weld pool collapses (Fig. 4) during welding of 4th and 5th welds. In addition, the 4th and 5th welds are not easy to fill. Therefore, the welding test is not completed. Analysis shows that the reasons for failure of groove A mainly include three aspects: (1) The gap between 316L and L415 is too large due to welding, which causes the filler metal to flow into the gap. Thus, the filler metal in the weld is insufficient, and the weld is difficult to fill. (2) Due to the existence of the gap, when 316L is completely melted, there is no solid metal supporting the molten pool, which causes the molten pool to collapse instantly. (3) Due to the deformation of the test couple, the precise dimensions of the machined groove cannot be guaranteed, and the height of the blunt edge at each point is greatly different, resulting in large amount of misalignment.

Groove A is improved, and groove B is designed. The advantages of groove B also lie in two aspects. On one hand, this groove can completely avoid the contact between the root weld (1st) and 316L, thereby reducing the welding difficulty. On the other hand, there are two weld paths for the 4th weld layer. This can play the role of seal welding which improves the welding efficiency and avoids the welding defects at the gap between L415 and 316L to a certain extent. But because the stainless steel wire is used for 4th and 5th weld bead, the production costs are higher than that of groove A. Figure 5a, b shows the macroscopic morphology of inner capping weld (after 5th weld layer) and outer capping weld (after 6th weld layer), respectively. It can be seen that the weld appearance is good. But RT result shows that the continuous incomplete fusion is observed at the corners of 4–2 weld bead (Fig. 5c). The reason is that, the 4–2 weld bead is narrow and deep, so the welding wire with diameter of 2.4 mm is not easy to fill. Although some measure has been taken, such as the weld bead is melted before welding of 4–2 weld bead by the arc without filling the welding wire to trim the shape of the previous weld, the defect of incomplete fusion remains. Due to the presence of incomplete fusion resulted by narrow and deep weld bead of 4–2, the groove B failed.

Based on groove B, groove C is designed. For groove C, it is also convenient for welding 316L layer, reducing the usage of filling materials and controlling the production costs. But there are two questions that should be paid attention to during sealing welding. On one hand, the welding current should be small to reduce the fusion ratio and welding heat input. This can avoid the gap expansion caused by different shrinkage ratios between 316L and L415. On the other hand, the sealing thickness should not be too large to cause trench which is not conducive to filling later. Besides, the back shape of root weld (3rd) depends on the actual welding condition, but the convex surface which may lead to the generation of trench should be avoided. Figure 6a, b shows the macroscopic morphology of sealing weld. As can be seen, the sealing weld is too wide, which will cause the root weld (3rd) to contact the sealing welds, resulting in the generation of hardened microstructure and the dilution of the alloy elements. This affects not only the mechanical properties but also the corrosion properties of welded joints. The reason why the sealing weld is too wide is that, the sealing weld is located at the V-shaped groove slope of 316L, and the welding operation is difficult to control. Therefore, after sealing welding, further welding test is abandoned.

Groove C is further improved, and groove D is designed. For groove D, there are two issues to note. On one hand, the root weld (3rd) of L415 layer should avoid contact with the sealing welds (1st and 2nd). On the other hand, the welding current of filler and cap welding of 316L layer should be small to reduce the welding heat input and prevent the sealing weld from remelting which can produce the defects. As shown in Fig. 7a, the sealing weld toe is far away from the groove boundary, which guarantees the isolation of the root weld (3rd) and the sealing weld (1st and 2nd). As can be seen in Fig. 7b, there is no fusion phenomenon between the root weld (3rd) and the sealing weld (1st and 2nd) after the weldment group. Figure 7c shows that the capping weld appearance of 316L layer is good. RT result illustrates that there are no welding defects (Fig. 7d).

In summary, the advantages of groove D are as follows: (1) The sealing welding has been used to avoid the weld pool collapse caused by the gap between 316L and L415 (problem with groove A). (2) The stripped length of 316L is large. This can avoid the presence of incomplete fusion resulted by narrow and deep weld (problem with groove B) and the contact of root weld of L415 with sealing weld (problem with groove C) and makes sealing welding easy to operate. Therefore, groove D and two kinds of welding materials (309MoL and 309L) have been adopted for butt welding L415/316L pipes.

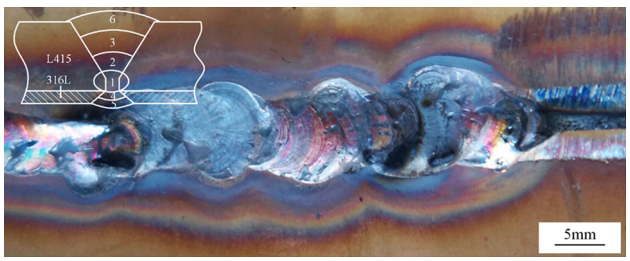

Fig. 4 Weld pool collapse after 4th and 5th weld bead of groove A

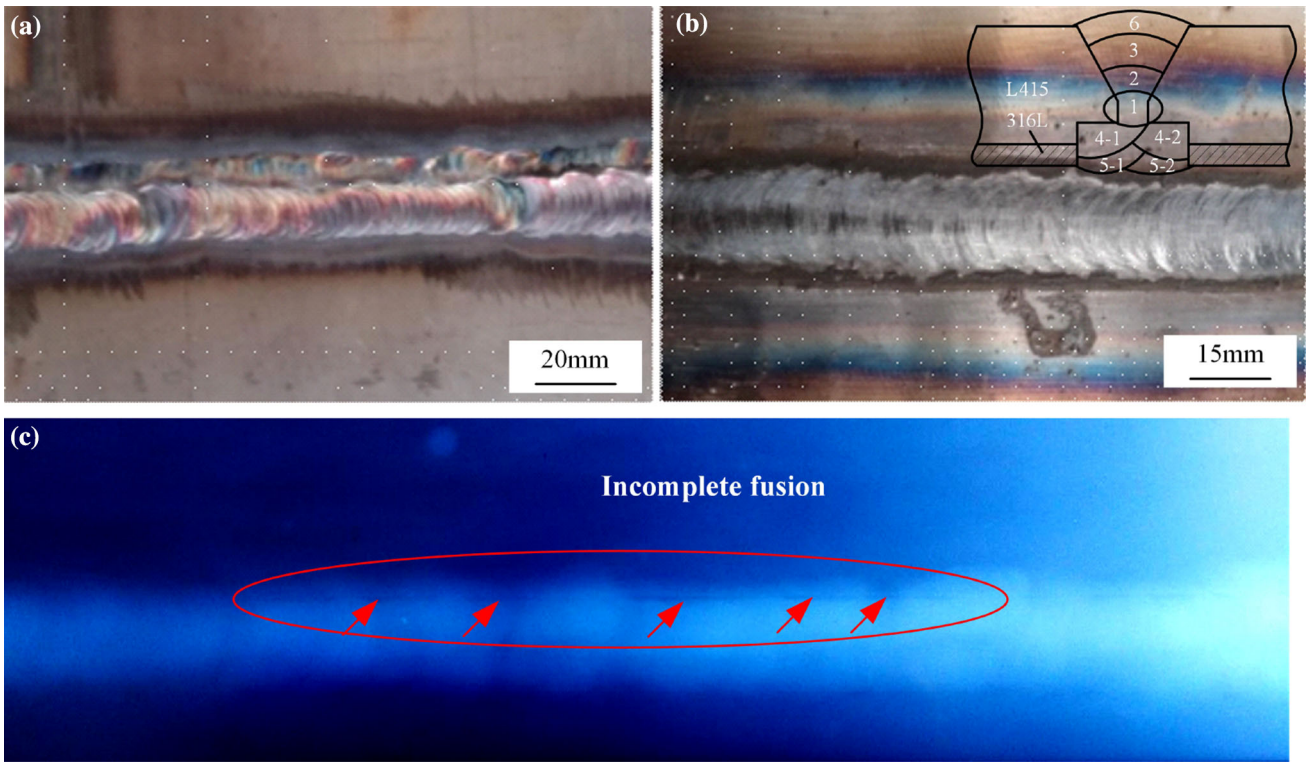

Fig. 5 Results of groove B **a** macroscopic morphology of inner cap weld; **b** macroscopic morphology of outer cap weld; **c** RT result

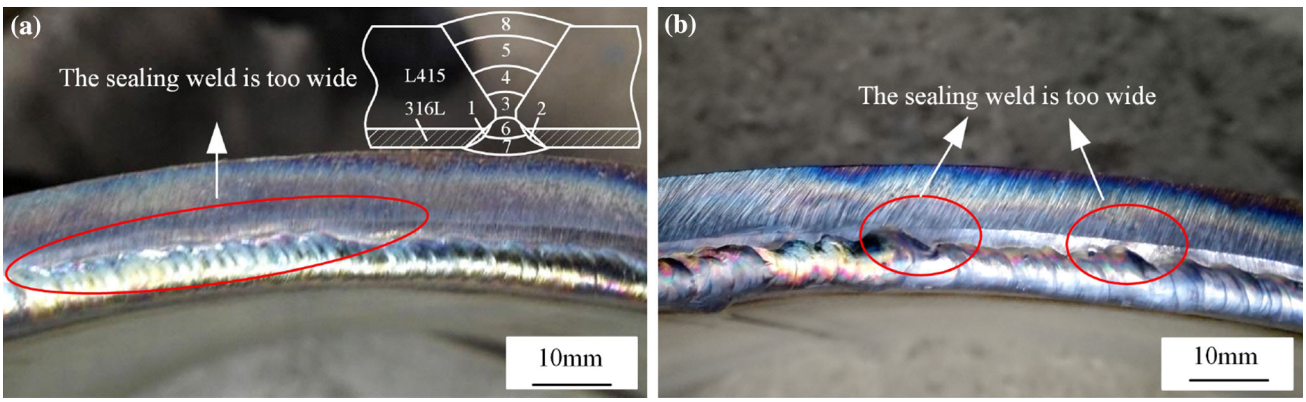

Fig. 6 Results of groove C **a** and **b** macroscopic morphology of sealing weld

3.2 Mechanical Properties

3.2.1 Tensile Test

Stress–displacement curves of tensile specimens are shown in Fig. 8. In this case, the stress is equal to the tensile force/area, and here the area is approximately equal to the actual width × thickness. The displacement equals the displacement at the clamping ends. As can be seen in Fig. 8, the four curves have similar trend. There is no obvious elastic deformation stage and yield stage.

The tensile specimens after test are shown in Fig. 9. It is found that the fracture of each specimen is located at L415, and there is an obvious necking phenomenon. The tensile data are shown in Table 5. The tensile strength of L415 is 520 MPa, and that of 316L is 480 MPa. The tensile strengths of welded joints using 309MoL and 309L are 581.5 MPa and 583 MPa, respectively. Also, the section shrinkage rates of 309MoL and 309L are 67.06% and 71.01%, respectively. This shows that the welded joints have high strength and excellent toughness. The fractographs of tensile specimens are shown in Fig. 10. As can be seen in Fig. 10a, b, the microfracture of 309MoL is

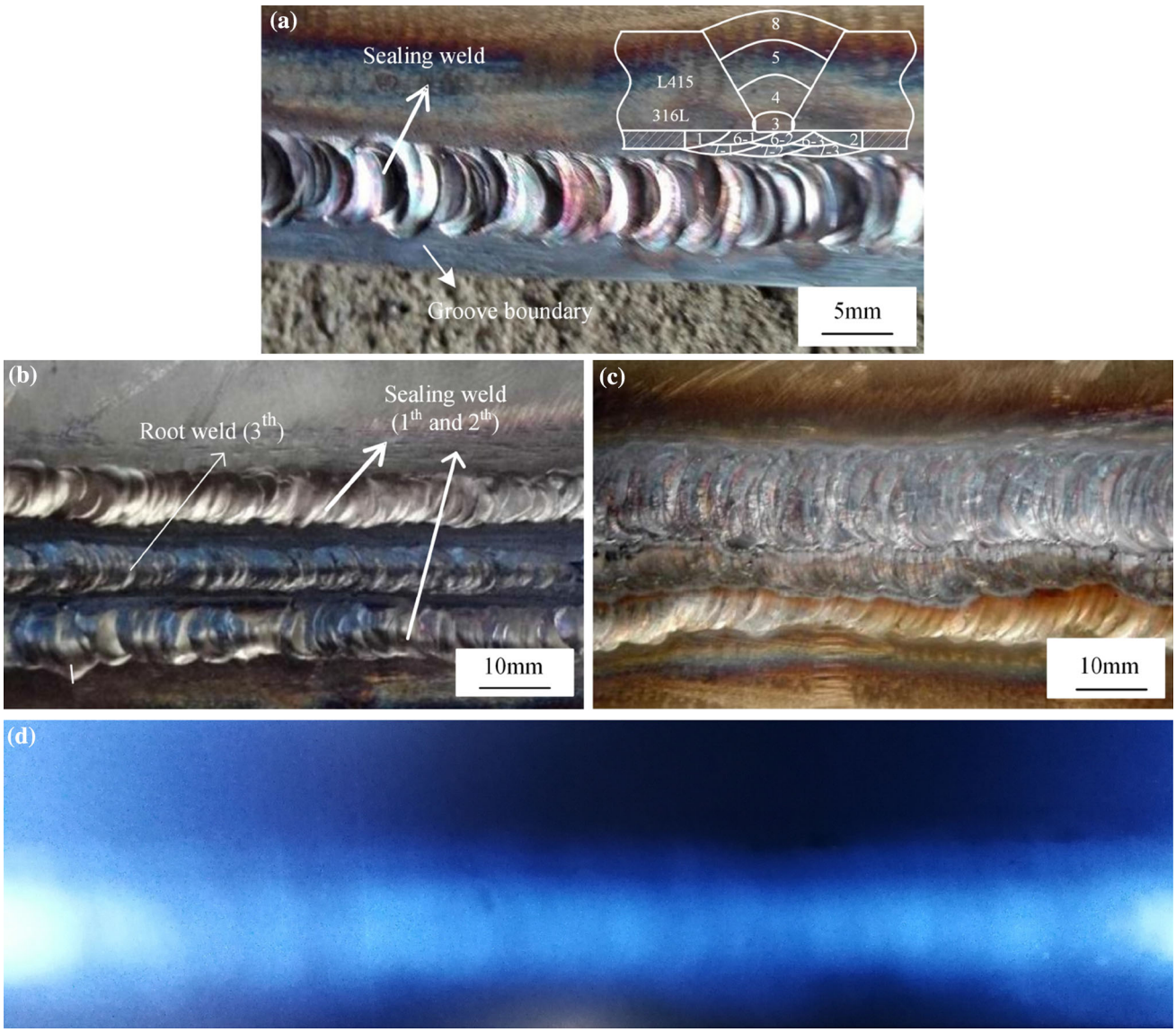

Fig. 7 Results of groove D macroscopic morphology of sealing weld **a** before and **b** after weldment group; **c** macroscopic morphology of 316L layer after welding; **d** RT result

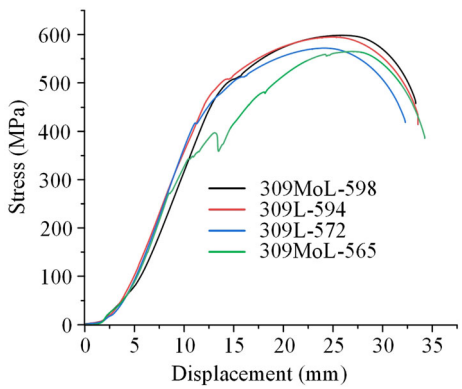

Fig. 8 Stress–displacement curves of tensile samples

similar to that of 309L, and shear planes are formed at 45° in the tensile axis direction. There are a large number of dimples in L415, which proves that the tensile fracture mode is ductile (Fig. 10c, d).

3.2.2 Bending Test

The bending specimens after test are shown in Fig. 11, and the data are shown in Table 6. It is found that no crack is formed on the four specimens using 309MoL (Fig. 11a) and the No. 1 and No. 4 specimens using 309L (Fig. 11b). A crack with a length of 1 mm is found on the No. 2 specimen. Meanwhile, two cracks with lengths of 1.95 mm and 1.28 mm appear on the No. 3 specimen (Fig. 11b). But the bending performance of the welded joints using both

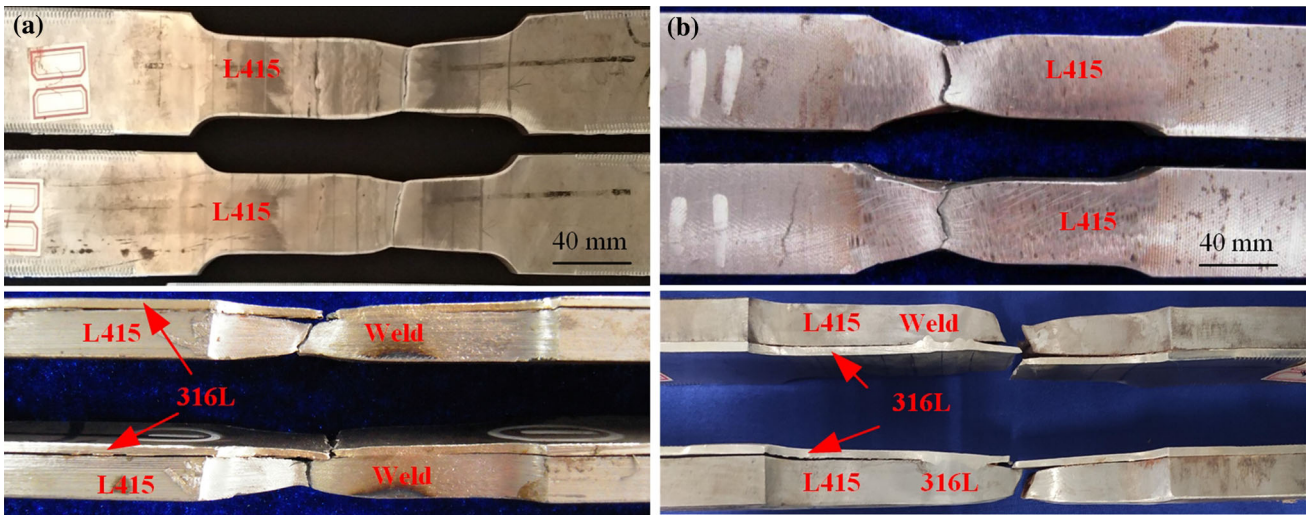

Fig. 9 Macromorphology of tensile specimens **a** 309MoL; **b** 309L

Table 5 Data of tensile test

Welding materials	Section shrinkage rate A/%	Tensile strength R_m/MPa
309MoL	67.6 (68.91, 65.21)	581.5 (565, 598)
309L	71.01 (69.57, 72.44)	583 (572, 594)

(1) Section shrinkage rate $A = (S_1 - S_0)/S_0$; (2) tensile strength = maximum tensile force/S_0; (3) S_1 is approximately equal to the actual width × thickness after test, and S_0 is approximately equal to the actual width × thickness before test

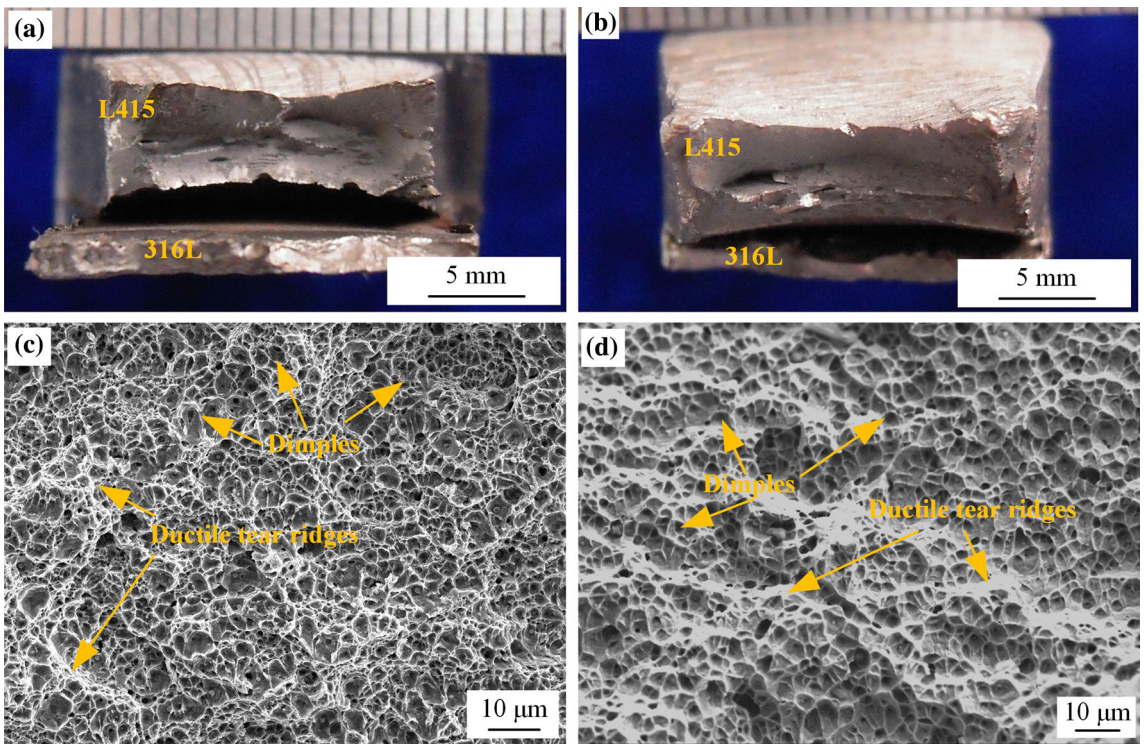

Fig. 10 Fractographs of tensile samples **a** macrofracture of 309MoL; **b** macrofracture of 309L; **c** microfracture of 309MoL; **d** microfracture of 309L

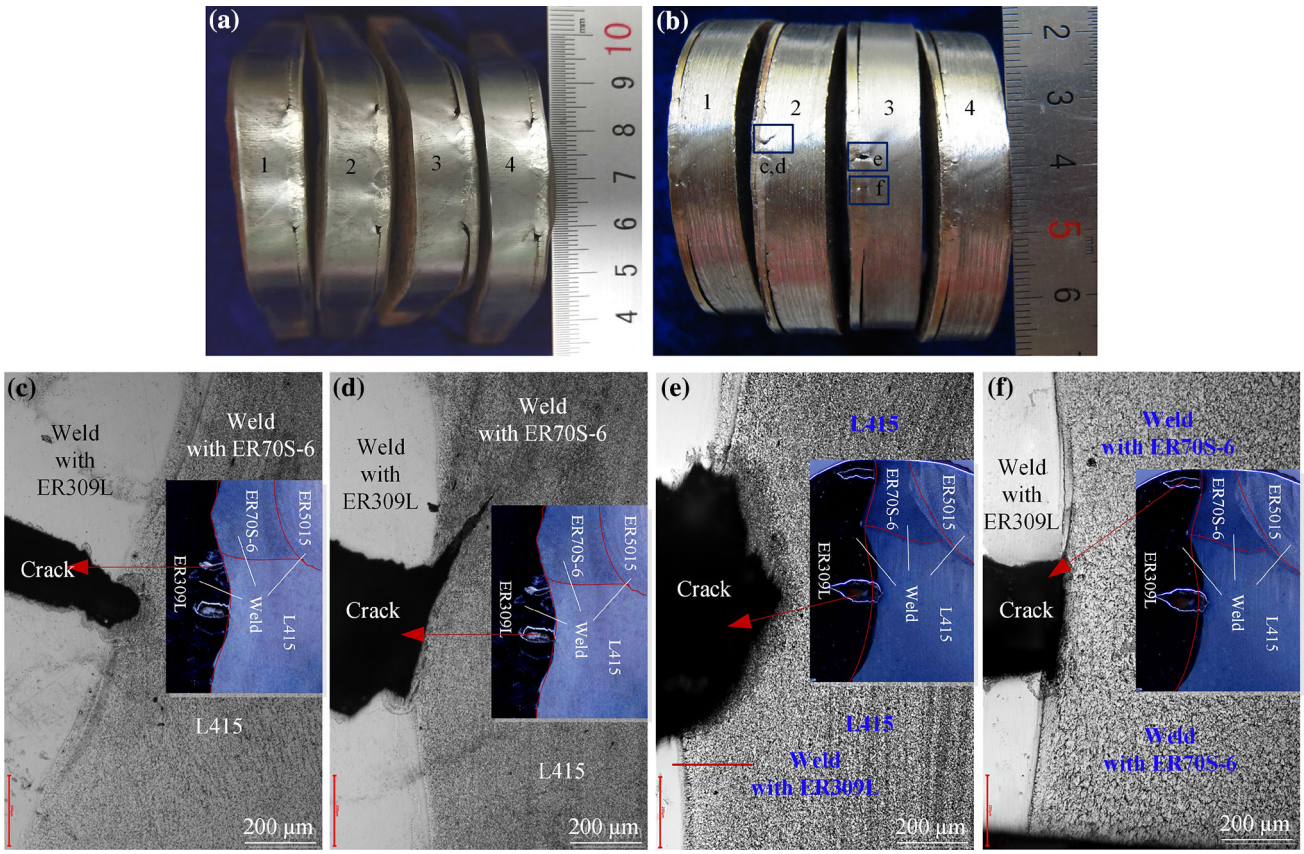

Fig. 11 Side-bending specimens and cracks macromorphology of 309MoL (**a**) and 309L (**b**); **c** and **d** cracks on No. 2 specimen of 309L; **e** and **f** cracks on No. 3 specimen of 309L

Table 6 Data of bending test

Specimen No.	309MoL-1	309MoL-2	309MoL-3	309MoL-4	309L-1	309L-2	309L-3	309L-4
Crack length/mm	0	0	0	0	0	1	1.95 1.28	0

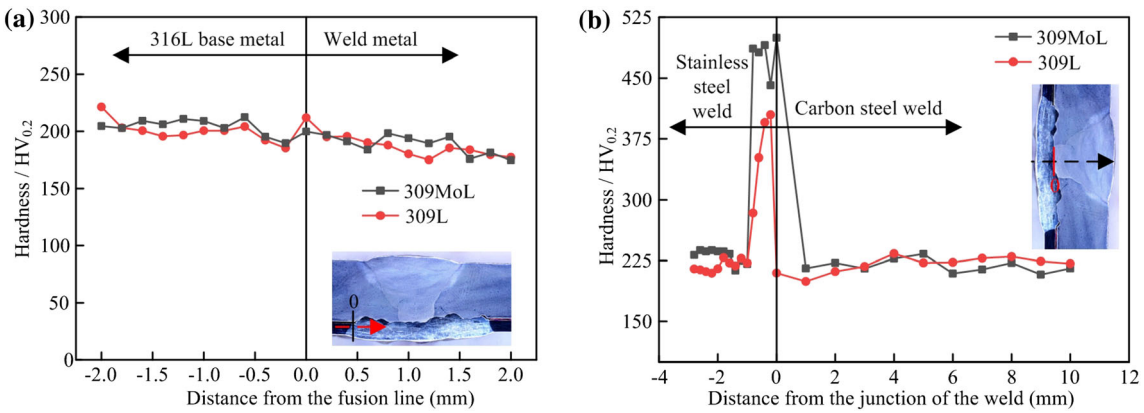

Fig. 12 Hardness distribution of welded joints **a** at the fusion line of stainless steel weld; **b** in vertical direction of welded joint

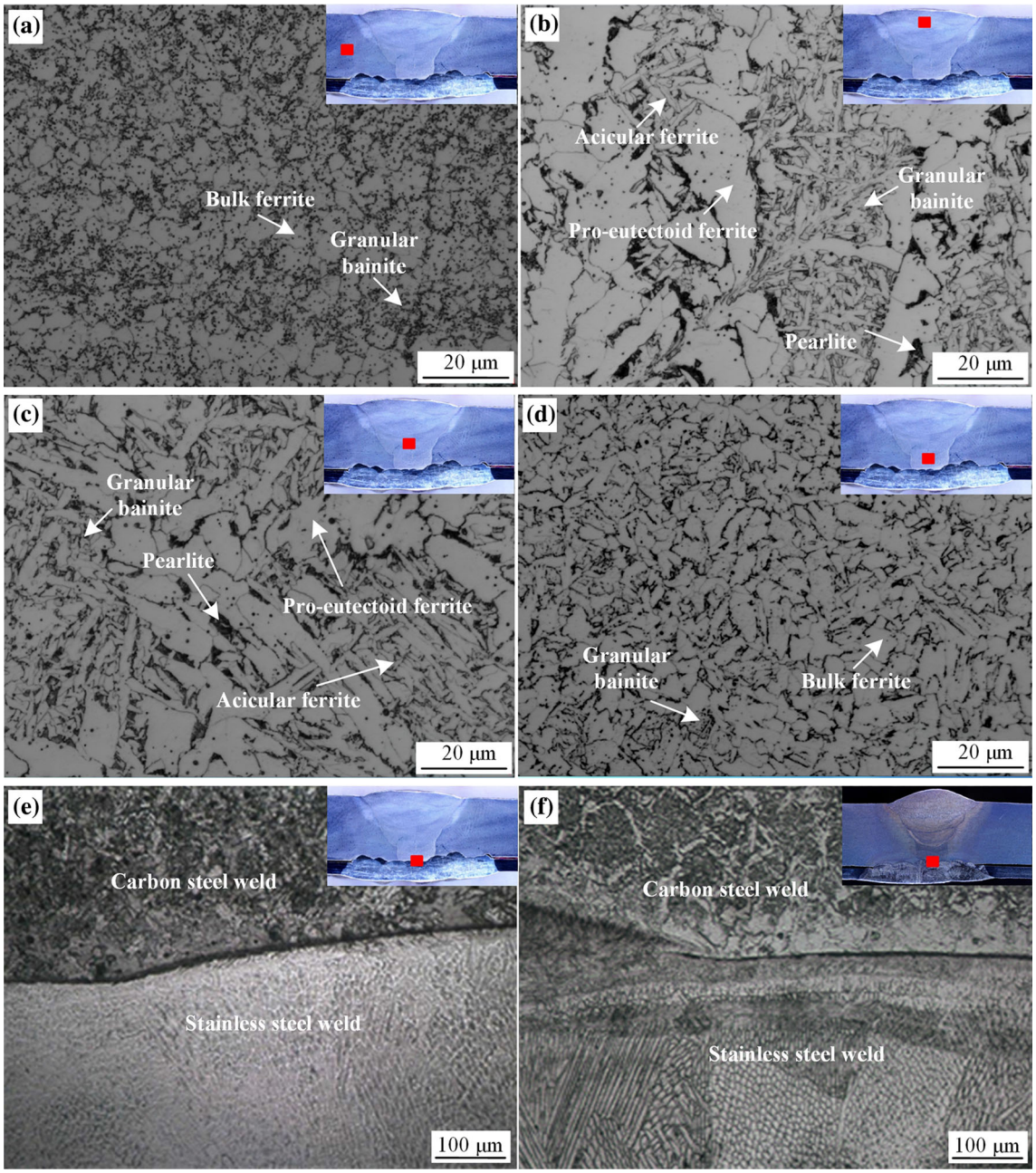

Fig. 13 Optical micrographs of welded joints **a** L415; **b** capping weld of L415; **c** filler weld of L415; **d** root weld of L415; junction of carbon steel weld and stainless steel weld of 309MoL **e** and 309L **f**; fusion zone between weld and 316L of 309MoL (**g**) and 309L (**h**); stainless steel weld of 309MoL (**i**) and 309L (**j**)

309MoL and 309L can all qualify the standard requirement of each crack length less than 3 mm. As observed in Fig. 11c, d, there are two cracks on the No. 2 specimen of 309L, but the small crack, which may exist under the stretched surface and appear after the preparation of the metallographic sample, cannot be found in Fig. 11b. In addition, as can be seen in Fig. 11c–f, the cracks appear at the weld junction between the root bead of L415 layer (weld with ER70S-6) or L415 and ER309L weld. Hardness test and EBSD have been used by the authors to analyze the causes of cracks [22]. The results show that the cracks on the bending specimen are closely related to the martensite formed at ER309L/ER70S-6 or ER309L/L415 interface, and martensite appear in the filler weld of ER309L (6th bead).

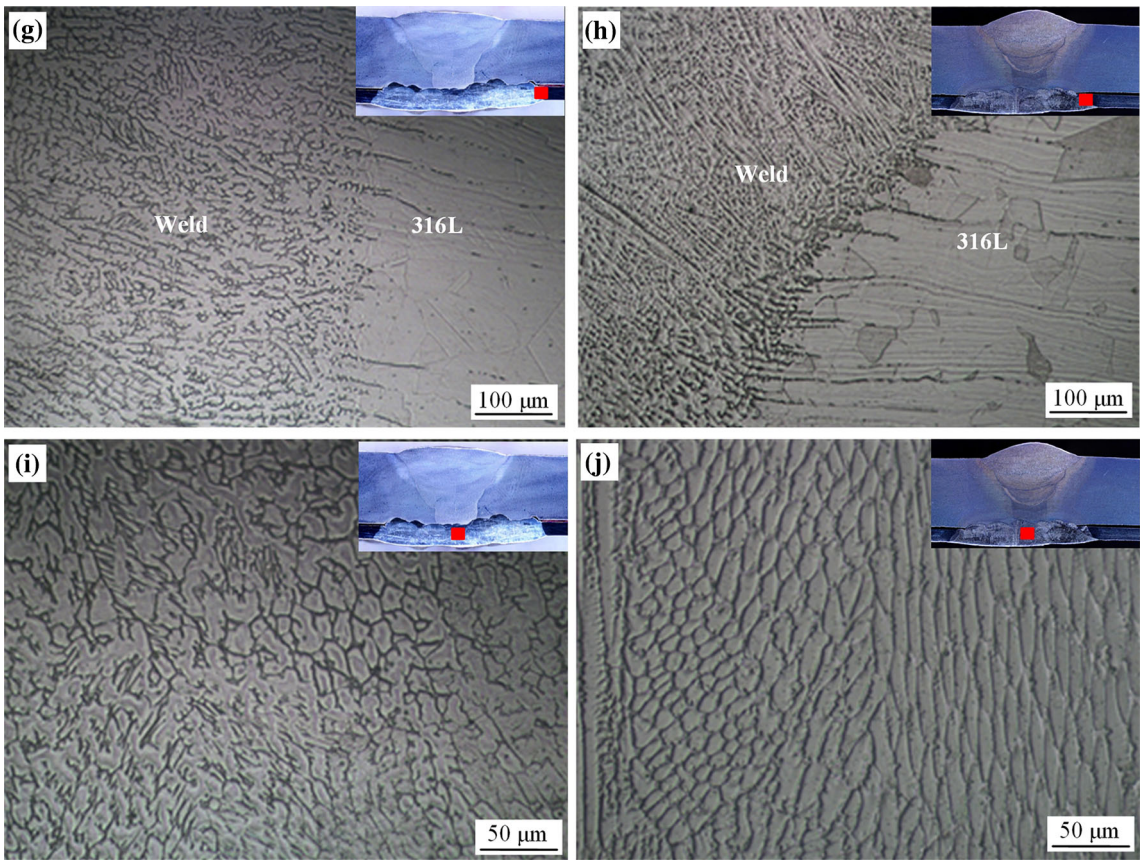

Fig. 13 continued

3.2.3 Hardness Test

Figure 12a shows the hardness distribution across the fusion zone between 316L and the weld. It is obvious that two curves have the same trend whether 309MoL or 309L is used. The hardness of 316L is slightly higher than that of the weld, the hardness near the fusion zone is not significantly increased, and a slight softening occurs in the range of about 0.6 mm on the side of 316L. This means that the selection of 309MoL and 309L welding materials are equal-strength matching. The reason for that the hardness of 316L is higher than that of the weld is mainly that the carbon content of 316 l is higher than that of the welding wire ER309L/ER309MoL. A slight softening occurs on the side of 316L because the welding process has an effect of post-weld heat treatment (PWHT) on 316L [23, 24], resulting in the coarser grain size and lower hardness of HAZ on the side of 316L.

Figure 12b shows the hardness distribution in the vertical direction of the weld center. It is found that two curves also have the same trend whether 309MoL or 309L is used. In the range of about 0.6–0.8 mm at the weld junction of stainless steel weld (3rd) and carbon steel weld (6th), the hardness value is abnormally high (the maximum values 499.50 $HV_{0.2}$ for 309MoL and 404.8 $HV_{0.2}$ for 309L), which will lead to poor toughness and welding defects such as crack during bending test (seen Fig. 11b). It is mainly due to the difference in the content of the alloy elements between the carbon steel welding material and the stainless steel welding material. In the transition layer, a decarburization layer occurs in the root weld (3rd) of carbon steel, and brittle structure of martensite exists in the stainless steel weld (6th) resulting in high hardness of the weld transition layer.

3.3 Microstructure Analysis

Figure 13 shows the optical micrographs of welded joints. The microstructure of L415 is bulk ferrite and granular bainite (Fig. 13a). The capping weld of L415 contains a lot of acicular and pro-eutectoid ferrite, and a small amount of pearlite (Fig. 13b). The filler weld of L415 is mainly composed of polygonal ferrite and granular bainite, and a small amount of pearlite and acicular ferrite (Fig. 13c). Figure 13d shows that the root weld of L415 mainly contains bulk ferrite and granular bainite. By comparing

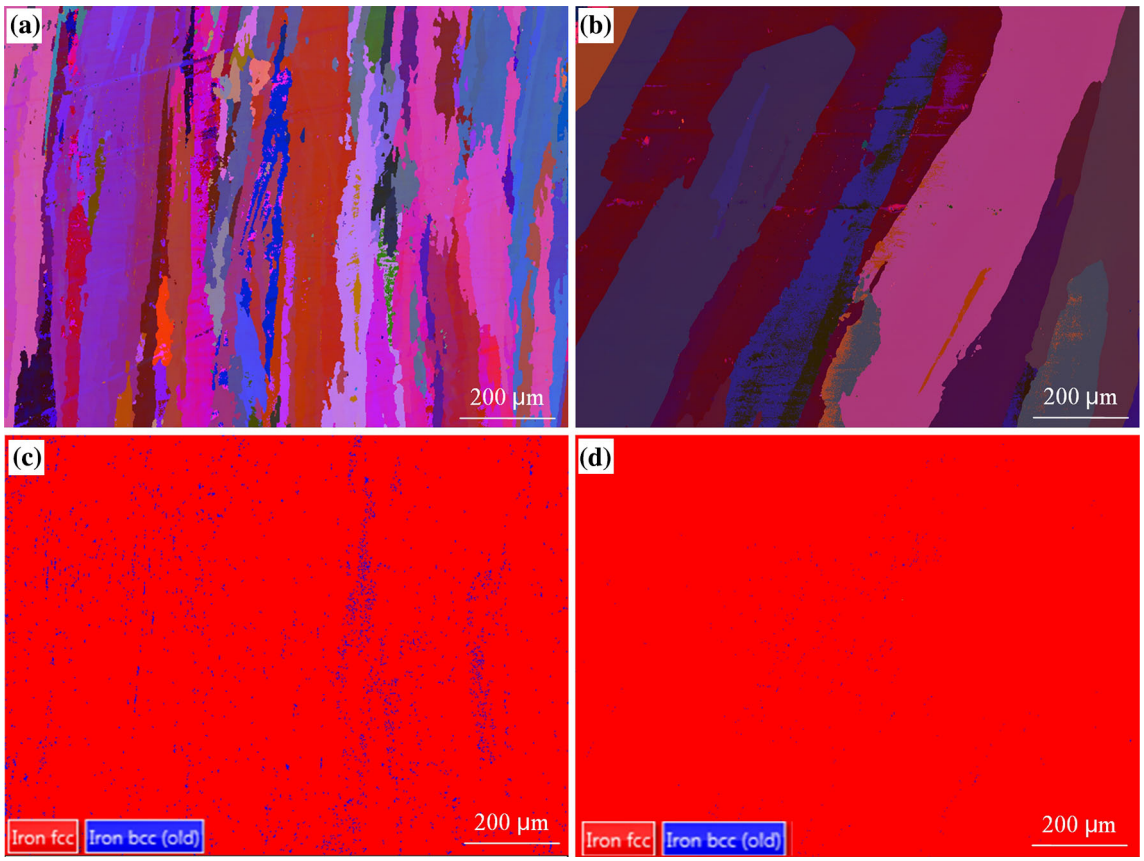

Fig. 14 EBSD graphs of capping weld of 316L **a** Euler graph of 309MoL; **b** Euler graph of 309L; **c** phase graph of 309MoL; **d** phase graph of 309L

Fig. 13a–c, it can be seen that the grain size of the root weld is smaller than that of the filler and capping weld due to the low small welding heat input, and the grain size of the filler weld is smaller than that of the capping weld because the latter has the effect of heat treatment on the former. Figure 13e, f depicts the microstructure of the junction of carbon steel weld and stainless steel weld of 309MoL and 309L, respectively. It is observed that microstructures of the both are similar. There is a clear decarburization layer on the carbon steel side and a narrow transition layer on the stainless steel side. In combination with hardness analysis (Fig. 12b), the transition layer should be martensite. Figure 13g, h shows the microstructure of fusion zone between the weld and 316L of 309MoL and 309L, respectively. It is obvious that the columnar dendrites in weld grow perpendicular to the fusion zone. The microstructures of the weld with both 309MoL and 309L are mainly cellular dendrites (Fig. 13i, j). Since both 309MoL and 309L are austenitic welding materials, the weld is austenite, and the effect of the welding materials on the microstructure is not visible.

Figure 14 shows EBSD graphs of capping weld of 316L. It can be seen that the grain size of 309MoL (Fig. 14a) is smaller than that of 309L (Fig. 14b). The reason is that, the element Mo is a carbide-forming element and hinders austenite grain growth. Figure 14c, d shows the EBSD phase graphs of 309MoL and 309L with blue and red indicating BCC and FCC phases, respectively. It can be found that the capping weld of both 309MoL and 309L is composed of a large amount of FCC phase and a small amount of BCC phase. Because both 309MoL and 309L are the austenitic welding materials, the FCC phase is austenite, and the BCC phase may be ferrite. In addition, it is found that the BCC phase of 309MoL is more than that of 309L. The reason may be that the Mo is a ferrite stabilizing element.

3.4 Composition Analysis

The chemical composition of 316L and the weld is measured. The composition analysis position and analysis results are shown in Fig. 15. It can be seen that some elements with low content such as C, S and P cannot be

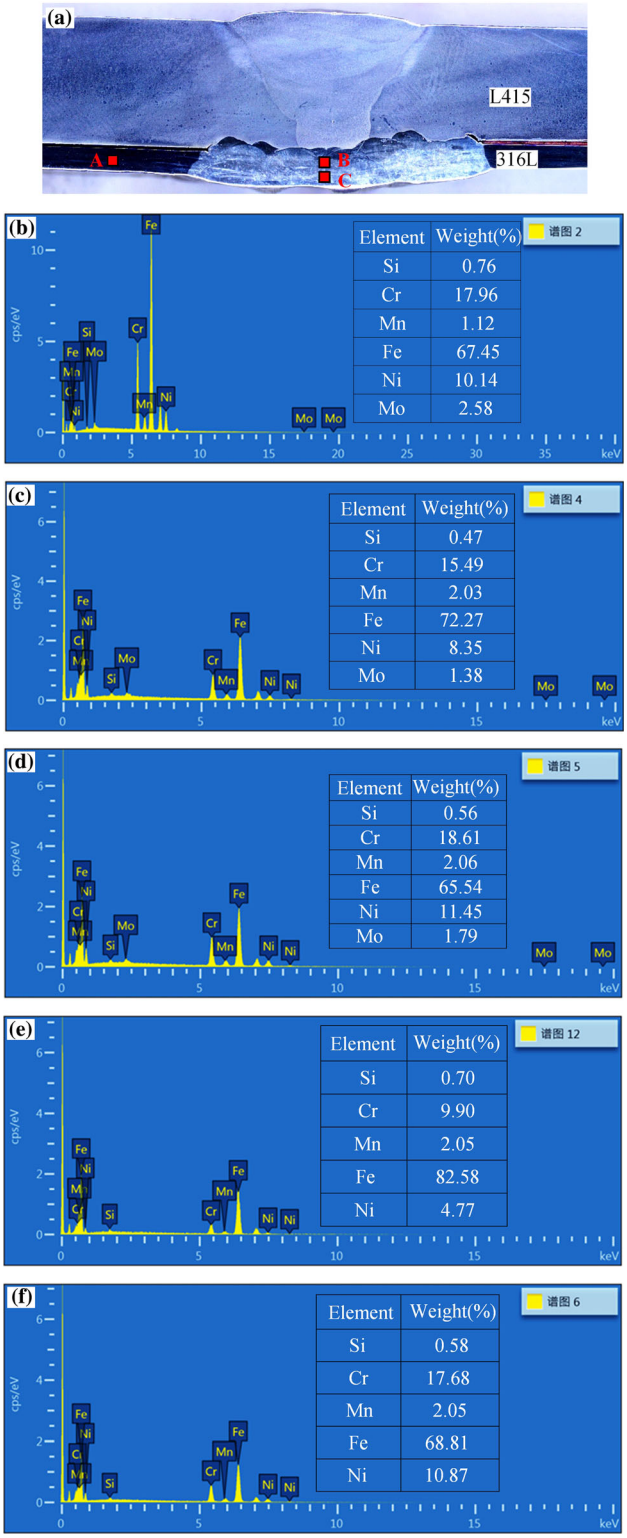

Fig. 15 Composition analysis position and EDS analysis results: **a** composition analysis position; **b** A spot of base metal 316L; **c** B spot and **d** C spot of weld of 309MoL; **e** B spot and **f** C spot of weld of 309L

detected. But the content of major alloying elements of 316L is similar to that illustrated in Table 1. There are not much different in the contents of Si and Mn in the two welds between point B (Fig. 15c, e) and C (Fig. 15d, f). In addition, the content of Fe in the two welds at point B (Fig. 15c, e) is higher than that at point C (Fig. 15d, f). However, the contents of Cr and Ni in the two welds at point B (Fig. 15c, e) are lower than that at point C (Fig. 15d, f). The reason is that, point B is close to the root weld of L415, and the corresponding component of point B is diluted by the root weld of L415. Therefore, the chemical composition of point B is between the root weld of L415 and point C. Also, it is noted that there is no Mo in the weld using 309L.

3.5 Corrosion Resistance Analysis

Figure 16a, b shows the pitting specimens using 309MoL. It can be seen that there are no pitting holes in both the weld and base metal 316L. However, there are obvious pitting holes in the weld of pitting specimens using 309L (Fig. 16c, d), indicating that the pitting corrosion resistance of the weld is worse than that of base metal 316L. Chen et al. [19] have shown that adding 2–3% Mo in stainless steel can improve the local corrosion resistance of stainless steel in chloride medium because Mo can increase the density of the passivation film and make it favorable for the formation of repassivation film. Therefore, it can be concluded that the welding wire 309MoL can improve the corrosion resistance of L415/316L bimetal mechanical lined pipe in media containing Cl^- compared to the 309L welding wire.

4 Conclusions

1. In terms of weld appearance and welding operability, the groove D (L415 is V shape with angle of 60° and blunt edge of 1 mm and 316L is stripped 6–8 mm) is most suitable for butt welding of L415/316L bimetal mechanical lined pipes.
2. The effect of welding materials on the microstructure of the welded joints is not visible. The weld of both 309MoL and 309L is composed of a large amount of austenite and a small amount of ferrite. However, the presence of Mo can refine the grain size and increase the content of ferrite phase.
3. There are no cracks on the 309MoL bending specimens, while cracks are found on the 309L bending specimens which may be related to the large grain size. But the tensile and bending performances of the welded joints using both 309MoL and 309L do meet the standard requirements.

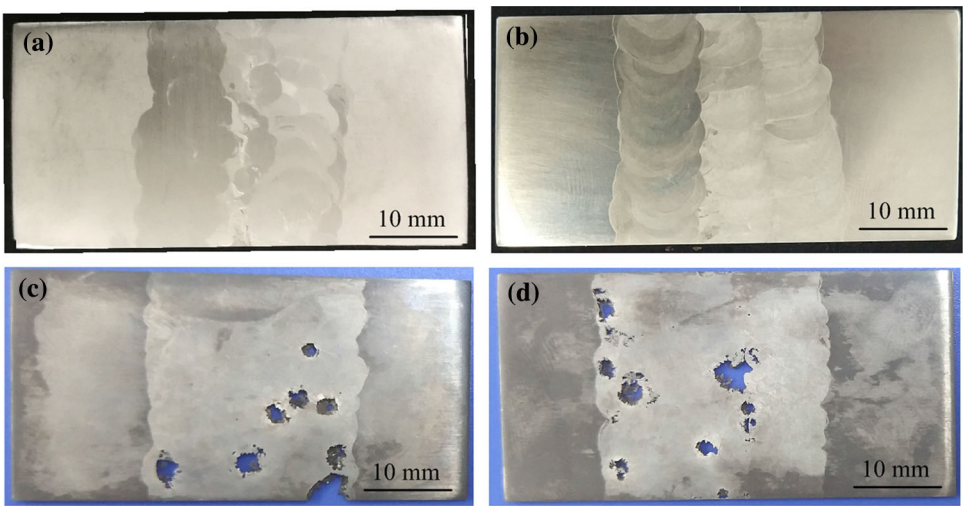

Fig. 16 Macroscopic morphology of pitting corrosion specimens **a** and **b** using 309MoL, **c** and **d** using 309L

4. Hardness test shows that the width of transition layer is about 0.6–0.8 mm at the weld junction of stainless steel weld and carbon steel weld, and the transition layer mainly contains martensite.
5. The effect of welding materials on the resistance to Cl^- corrosion is obvious. The welding wire 309MoL can improve the corrosion resistance of the weld compared to 309L.
6. The post-internal-welding process is suitable for butt welding of bimetal composite pipes.

Acknowledgements This work was supported by the Natural Science Foundation of Shandong Province (ZR2013EEQ027) and Key Technology Research and Development Program of Shandong (2016ZDJS05B03).

References

1. Rodionova I G, Rybkin A N, Poretskii S V, Stolyarov V I, and Baklanov O N, *Chem Technol Fuels Oil* **38** (2002) 67.
2. Song F M, *Electrochim Acta* **55** (2010) 689.
3. Kermani M B, and Morshed A, *Corrosion* **59** (2016) 659.
4. Wei B, Li H, and Li F, *Oil Gas Storage Transp* **35** (2016) 343.
5. Spence M A, and Roscoe C V, *Oil Gas J* **97** (1999) 80.
6. Chen W C, and Petersen C W, *SPE Prod Eng* **7** (1992) 375.
7. Serikov O, *Metallurgist* **49** (2005) 347.
8. Banse J, *Stainl Steel World* **10** (1998) 48.
9. Gou N N, Zhang J X, Zhang L J, Li Z G, and Bi Z Y, *Int J Adv Manuf Technol* **86** (2016) 2539.
10. Zhang L J, Pei Q, Zhang J X, Bi Z Y, and Li P C, *Mater Des* **64** (2014) 462.
11. Russell D K, and Wilhelm S M, *SPE Prod Eng* **6** (1991) 291.
12. Jiang W, Chen W, Woo W, Tu S T, and Em V, *Mater Des* **147** (2018) 65.
13. Jiang W, Luo Y, Zhang G D, Woo W, and Tu S T, *Mater Des* **51** (2013) 1052.
14. Han H, Han B, Li L Y, and Zhang S Y, *Electr Weld Mach* **47** (2017) 17.
15. Li L Y, Wang C, Han B, and Pu J T, *Trans Mater Heat Treat* **35** (2014) 125.
16. Huang B S, Chen Q, Zhao X, Zhang R F, and Zhu Y, *Trans Indian Inst Met* **71** (2018) 2933.
17. Liu D M, Han B, and Li L Y, *China Pet Mach* **44** (2016) 108.
18. Gou N N, Zhang J X, Wang J L, and Bi Z Y, *J Mater Eng Perform* **26** (2017) 1801.
19. Chen H, Ma H Z, Chen X M, Jiang S F, and Wang H J, *J Fail Anal Prev* **15** (2015) 563.
20. GB/T 9711.2-1999, Petroleum and natural gas industries-technical delivery conditions-parts 2: pipes of requirements class B.
21. GB/T 20878-2007, Stainless and heat-resisting steels-designation and chemical composition.
22. Li L Y, Xiao J, Han B, and Wang X L, *Int J Press Vessel Pip* (2019) https://doi.org/10.1016/j.ijpvp.2019.104026.
23. Pandey C, and Mahapatra M M, *J Mater Eng Perform* **25** (2016) 2761.
24. Pandey C, Mahapatra M M, Kumar P, and Saini N, *Mater Sci Eng A* **685** (2017) 39.